On the crystallographic, stage I-like, character of fine granular area formation in internal fish-eye fatigue cracks

Article *in* International Journal of Fatigue · September 2017

DOI: 10.1016/j.ijfatigue.2017.09.013

CITATIONS
7

READS
276

7 authors, including:

Andre Pineau
MINES ParisTech
364 PUBLICATIONS **9,903** CITATIONS

SEE PROFILE

T. F. Morgeneyer
MINES ParisTech
104 PUBLICATIONS **1,062** CITATIONS

SEE PROFILE

H. Abdesselam et al. Int. J. of Fatigue (2017), accepted : https://doi.org/10.1016/j.ijfatigue.2017.09.013

On the crystallographic, stage I-like, character of fine granular area formation in internal fish-eye fatigue cracks

H. ABDESSELAM[1, 2], J. CREPIN[1], A. PINEAU[1], A-L.ROUFFIE[2], P. GABORIT[3], L. MENUT-TOURNADRE[3], T. F. MORGENEYER[1*]

[1] MINES ParisTech, PSL Research University, Centre des Matériaux, CNRS, UMR7633, BP 87, 91003 Evry Cedex, France

[2] Safran Tech, Pôle M&P, Rue des Jeunes Bois, Châteaufort, 78772 Magny les Hameaux, France

[3] Safran Aircraft Engines, Villaroche, Rond-Point René Ravaud-Réau, 77550 Moissy-Cramayel, France

***Thilo.morgeneyer@mines-paristech.fr**

Abstract

The crystallographic character of fine granular area (FGA) formation from internal particles in martensitic high strength steel has been revealed by an assessment of the plastic zone size at the FGA border. This plastic zone size corresponded to about 3 times the martensite lath width. Tests at different temperatures (20°C, 200°C and 400°C) revealed a decreasing FGA size with increasing temperature at constant applied stress amplitude. As a consequence, the critical stress intensity factor varied as the FGA decreased with temperature. In contrast, the critical plastic zone size remained constant and equal to the sizes of microstructural features. This represents a strong similarity between crystallographic, stage I-like, crack propagation and FGA formation in a vacuum.

Keywords: Fine Granular Area (FGA), Plastic zone, Stage I-like, VHCF, Optically dark area, Martensitic High Strength Steel

1. Introduction

The aerospace industry is constantly looking for new technologies that will meet the objectives of performance, safety and reduction of fuel consumption. High strength steels have become well suited for weight reduction and guaranteeing the reliability of structures for long term service. Large variability in fatigue life is often found for ultra-high strength steels **[1]**. This fact requires using high coefficients of security for structural design. S-N curves of these steels have a distinct knee point within the high cycle and the very high cycle fatigue regimes with a plateau between them. Experimental data can be divided into two characteristic failure types on non-metallic inclusions: surface fracture mode at higher stress level leading to fewer loading cycles and interior fracture mode at lower stress levels leading to very long fatigue lifetime **[2] [3] [4] [5]**. Thus, there is a stress level for which the crack initiation changes from the surface to the internal structure of the material, which is associated with substantially longer fatigue lives.

In the literature, interior crack-induced failure at low stress levels has been identified as being a typical failure mode of high strength steel in the gigacycle fatigue regime **[6]**. This mode has the particularity of forming ring-like patterns around particles initiating the crack and which is called 'fish-eye' **[7].** A fish-eye is formed during the transition of fatigue crack propagation under vacuum to air **[6]**. Mostly for very high cycle fatigue, it is possible to find inside the fish-eye a fine granular structure particularly rough and circular around particles, which is called FGA (Fine Granular Area) **[6]**. Several names have been given to this zone: ODA (Optically Dark Area), GBF (Granular Bright Facet) or also RSA (Rough Surface Area) **[3, 6-9]**. The formation of the FGA is expected to enhance the fatigue lifetime for internal cracks **[10]**. However, FGA is not systematically present and recent investigations have been carried out to explain its formation **[1, 11, 12]**. *Sakai et.al (2015)* and *Grad et al. (2012)* **[1, 11]** proposed a similar scenario where the FGA is formed in three stages: (i) formation of fine

granular layer, (ii) nucleation of microdebonding, and (iii) coalescence of microdebonds and complete formation of a fine granular area. *Shiozawa et al.(2006)* proposed a decohesion model **[8]**. According to them multi-microcracks can be initiated by decohesion of carbides from the matrix around an inclusion. The authors relate the roughness to the carbide size. *Murakami et al. (1999)* proposed a hydrogen embrittlement assisted cracking model. The rough surface formed around the inclusion is due to hydrogen embrittlement assisted fatigue crack growth according to **[13, 14]**. In addition, *Nakamura et.al*, suggest that FGA is not formed during the crack growth process but formed by long term repeating compressive loading after fatigue crack was generated **[15]**. *Spriestersbach et al., (2016)* succeeded in creating a FGA with fatigue tests with artificial surface defects performed in a vacuum **[16]**. Tests in air showed no FGA formation, the vacuum conditions seem to be crucial for slow crack propagation and FGA formation.

Furthermore, from a fracture mechanics point of view, non-metallic inclusions cause a local increase of the stress field during loading. Thus, a stress intensity factor can be estimated at the inclusion using *Murakami et.al (1999)* formula and also for each stage of crack propagation. Several studies have shown that formation of FGA occurs only below a constant K_{FGA} threshold around 6-7MPa$\sqrt{m}$ **[1, 17-20]**.

In summary, the FGA formation is not fully understood as several contradictory scenarios are suggested in the literature.

In the present study the fatigue crack initiation and propagation mechanisms were investigated to understand the difference between surface and internal crack initiation which lead to different fatigue lifetimes and in particular the mechanisms of the FGA formation. Fatigue tests for different temperatures were carried out and from quantitative SEM fractography observations, sizes of inclusions, FGA and fish-eye were measured for internal

fatigue crack initiation. The effect of particle nature on fatigue life has been assessed. Each stage of the micro-propagation of the crack was evaluated with threshold values of stress intensity factor range calculated from Murakami's equations **[7]**. Plastic zone sizes at FGA crack tip were calculated for different temperatures and were compared to microstructural features' sizes. A new scenario of FGA's formation is proposed.

2. Experimental procedures and material

2.1. Microscopy

Optical microscopy, scanning electron microscopy (SEM), electron backscattered diffraction (EBSD) and transmission electron microscopy (TEM) were used for microstructural characterization. The TEM observations were conducted using a TECNAI-F20 microscope operated at 200 kV essentially in a dark-field mode. Thin TEM foils were prepared for TEM analysis by electropolishing in a solution of butoxyethanol, perchloric acid, ethanol and water at 30V during 18s. The EBSD measurements were conducted using a field emission gun scanning electron microscope (FEG-SEM) instrument (FEI Nova NanoSEM450 S-FEG) operating at 15 kV. Orientation mapping for the FEG-SEM/EBSD data was performed with a 100 nm step size. TSL-OIM software was used for the orientation measurement and analysis. SEM observations were carried out using the same SEM instrument operating at 10 kV or less if suited. Optical images were obtained using a Leica DMI 5000 M microscope, after a few seconds of 2% Nital etching on the specimen.

2.2. Material

Material used in this study was X23NiCoCrMoAl 13-6-3, a maraging type of steel. Chemical composition and mechanical property of this steel is shown in **Table 1**:

Table 1: Chemical composition (wt %) and yield strength of the studied material

C	Cr	Mo	Co	Ni	Al	V	σ_y at 20°C (MPa)	σ_y at 400°C (MPa)
0.23	3.3	1.5	5.8	13.0	1.5	0.25	1990	1500

The microstructure of the steel was investigated. The results are presented in **fig.1** which identifies the sizes of microstructural entities. This will help to correlate the microstructure with the crack initiation and propagation mechanisms in fatigue.

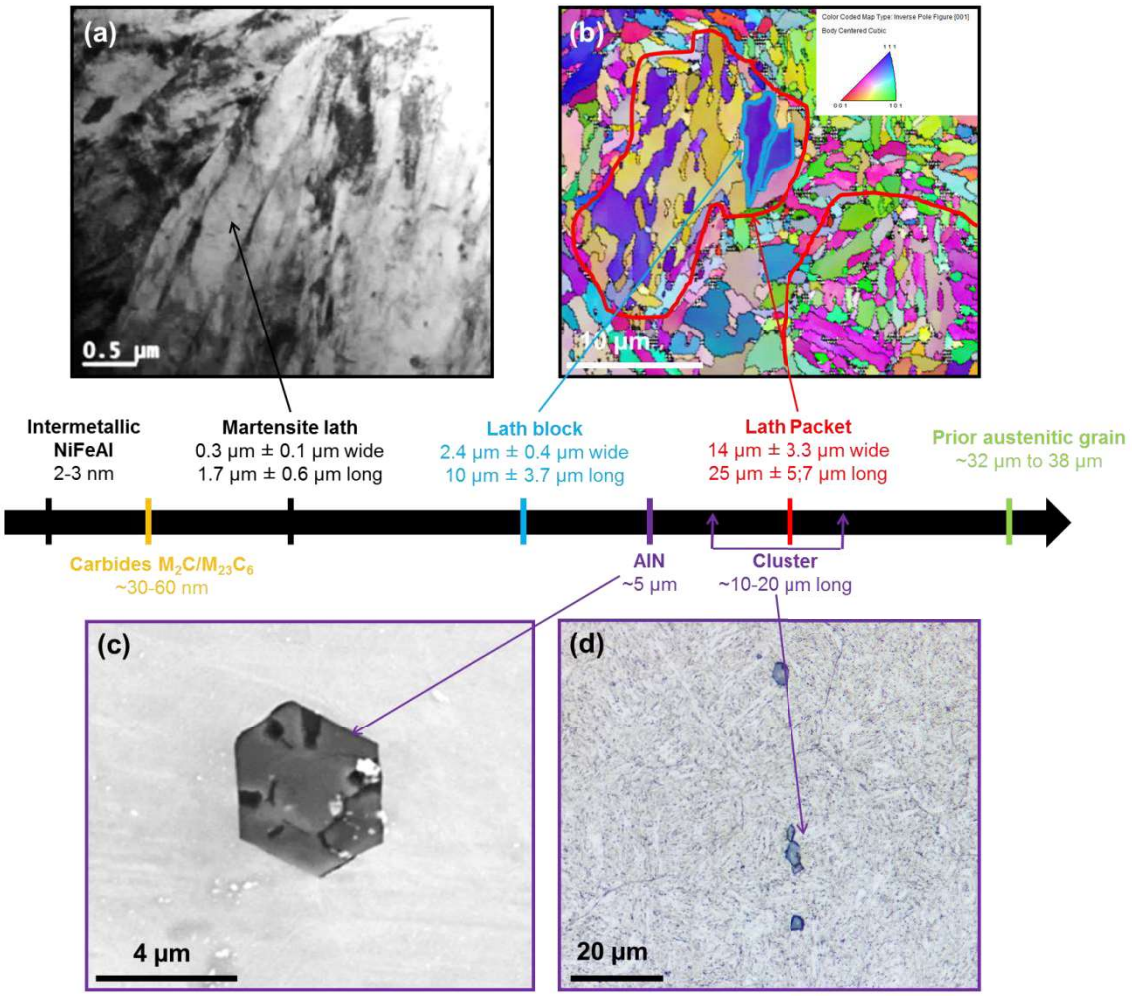

Fig. 1 Observations of the sizes of microstructural entities that can be found in the material:

(a) TEM image of martensite lath (b) Inverse pole figure (IPF) + Image quality (IQ) of an EBSD map with lath packet and lath block highlighted in red (c) SEM image of a non-metallic inclusion of AlN (d) Optical image of an AlN cluster after 2% Nital etching

The microstructure consisted of a martensitic matrix hardened by the co-precipitation of an intermetallic phase NiFeAl and secondary carbides M_2C. It also contained non-metallic inclusions such as aluminium nitrides (**fig.1 (c), (d)**) that could act as stress concentration sites when the steel was subjected to fatigue loads. The size and shape of these inclusions varied greatly depending on whether they were found in an isolated form or a clustered form. The matrix had a nested microstructure as described in *Kitahara et.al (2006)* **[21]** for low carbon martensitic steels. Martensite laths follow a three-level hierarchy in their morphology: martensite lath (**fig.1 (a)**), block and packet (**fig.1 (b)**). Martensite laths are 1 µm to 2 µm long and 200 nm to 400 nm wide. Blocks are made of martensite laths with the same crystallographic orientation. Their sizes approach 10 µm in length and 2.4 µm in width. Finally, packets are aggregations of several blocks. They have an anisotropic morphology with a 14 µm width and 25 µm length for the present material. All of those three level sub-structures were present in the original austenitic grain with a size of 38 µm.

2.3 Fatigue testing

Fatigue tests were performed according to ASTM norms E606 and E644 under tension-tension axial loading either under strain control ($R\varepsilon=\varepsilon_{min}/\varepsilon_{max}=0$) at a frequency of 1Hz or stress control ($R\sigma=\sigma_{min}/\sigma_{max}=0$) at 10Hz to 60Hz using an electro-servo-hydraulic testing machine and Ø 4.37 mm cylindrical specimen. Considering that the maximum stress was far below the yield stress and that no cyclic stress relaxation was observed, the macroscopic

behavior remained elastic and strain control or stress control tests are considered as equivalent ($R\sigma=R\varepsilon=0$). Both kinds of results are shown in the same data base for the present analysis. Fatigue lives are crucial and samples are ranked in terms of fatigue life. The measured maximum stress level has been used for LEFM calculations. The fracture surfaces of specimens which failed in fatigue were imaged and analyzed with the FEG-SEM instrument described above.

All the characteristic fracture surface regions were measured in the SEM to determine the following:

(a) Localization of the crack initiation and then the fracture mode (surface/internal)

(b) Distance of the crack initiation from the specimen surface

(c) Feret diameters of the inclusion leading to crack initiation were determined. Note that the Feret diameter corresponded to the distance between the two furthest points of the inclusion measured in a given direction. The maximum value of Feret diameter was measured in the direction corresponding to the inclusion's length. The inclusion width was perpendicular to this length direction. The inclusion area could be calculated with these two measures **[22]**.

(d) For internal crack initiation mode: (i) Presence of an FGA and Feret diameters (ii) Fish-eye diameter

(e) End of the fatigue crack growth and the distance from the crack initiation

3. Experimental results and discussion

3.1 Scenarios of surface and internal crack propagation

SEM fractography observations were carried out in order to investigate the internal and surface crack initiation mechanisms at two temperatures (20°C and 200°C) and at two maximum stress levels (~1300 MPa and ~1450 MPa). Specimens were selected at a stress level where there was a competition between surface and internal crack initiation.

Two scenarios of crack initiation mechanisms could be identified as shown in **fig. 2** and **fig. 3**: For the first case scenario, i.e. surface crack initiation (**fig. 2**): The crack initiation on a surface inclusion led to crack propagation in air until the stress intensity factor of the crack reached the limit of toughness of the steel. For the second case scenario, internal crack initiation (**fig. 3**) leads to the formation of a fine granular area around the initiation site. The crack then propagates under vacuum with formation of a fish-eye and finally propagates in air outside the fish-eye until the limit of toughness is reached. The final ductile fracture is a cup cone fracture with shear lips at the specimen surface. This scenario can be resumed in five steps:

1) Interior crack initiation on an inclusion
2) FGA formation (for some cases)
3) Crack propagation in vacuum with a fish-eye formation
4) Crack propagation in air
5) Final rupture

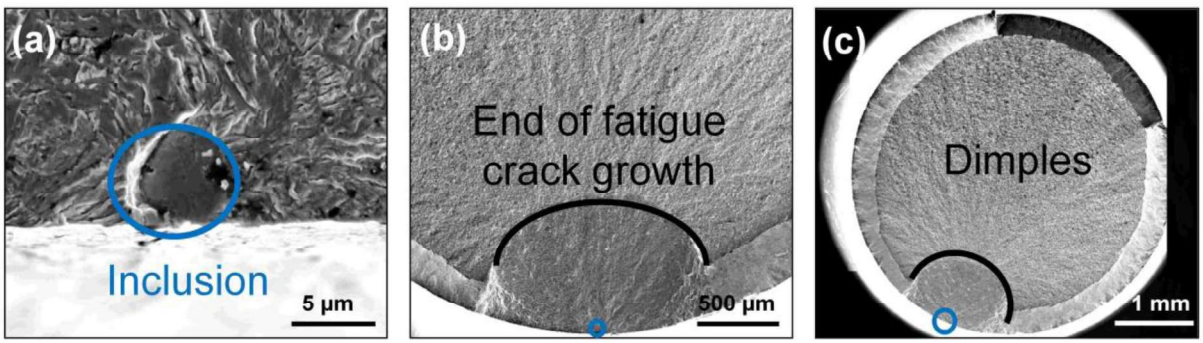

Fig.2. Surface crack initiation scenario: SEM images of a fatigue fracture (σ_{max} ~1450 MPa, T=20°C, cf: Fig 6 specimen n°8) with (a) Crack initiation at an inclusion at the specimen surface (b) Crack propagation in air with the end of fatigue crack growth (c) full fracture surface with ductile dimple failure region of the specimen

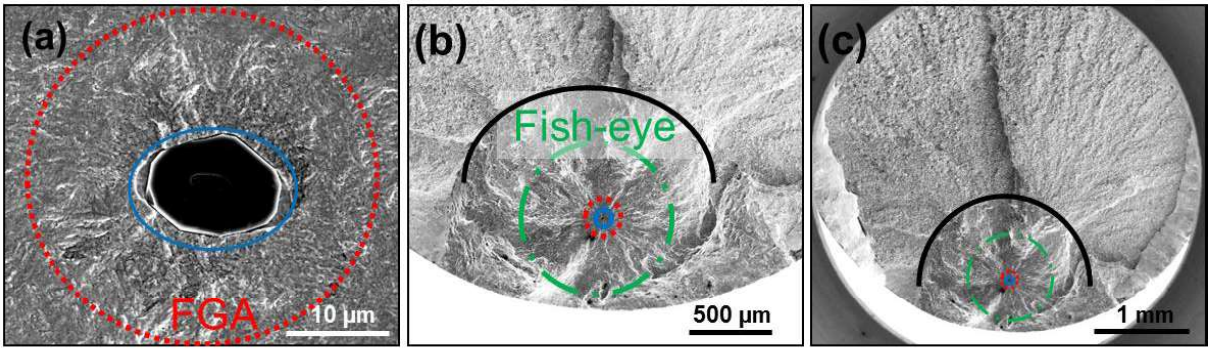

Fig.3. Internal crack initiation scenario: SEM images of a fatigue fracture (σ_{max} ~1450 MPa, T=20°C, cf: Fig 6 specimen n°21) with: (a) Crack initiation at an inclusion and the (potential) formation of a fine granular area (FGA) (b) Crack propagation under vacuum with the formation of a fish-eye (c) Crack propagation in air with the end of fatigue crack growth indicated in black

The scenario of internal crack initiation presents two more crack propagation stages than the surface initiation mode: FGA formation and fish-eye formation was also found in **[6]**. Those stages were sufficient to produce a large variability in the fatigue lifetime between surface and internal initiation modes when the fatigue crack propagation rates were different between the different crack propagation stages **[23]**. It should be noted that the FGA formation and fatigue crack propagation in air were not found for some specimens as will be discussed later.

3.2 Analysis of crack initiating particles

From the fractography observations it was found that fatigue cracks systematically initiated from non-metallic inclusions. **Fig.4** shows SEM images of different morphologies of inclusions leading to crack initiation in fatigue. The morphologies of inclusions have been classified in three categories in this study: (**fig.4 (a)**) isolated inclusion: it corresponds to an isolated inclusion, an aluminium nitride; (**fig.4 (b)**) Broken particle: it is an isolated inclusion which was broken during the elaboration of the steel which can be seen on the fracture surface as there is steel matrix present between the different parts of the particle; (**fig.4 (c)**) Cluster: it is a group of fragments of inclusions near to each other.

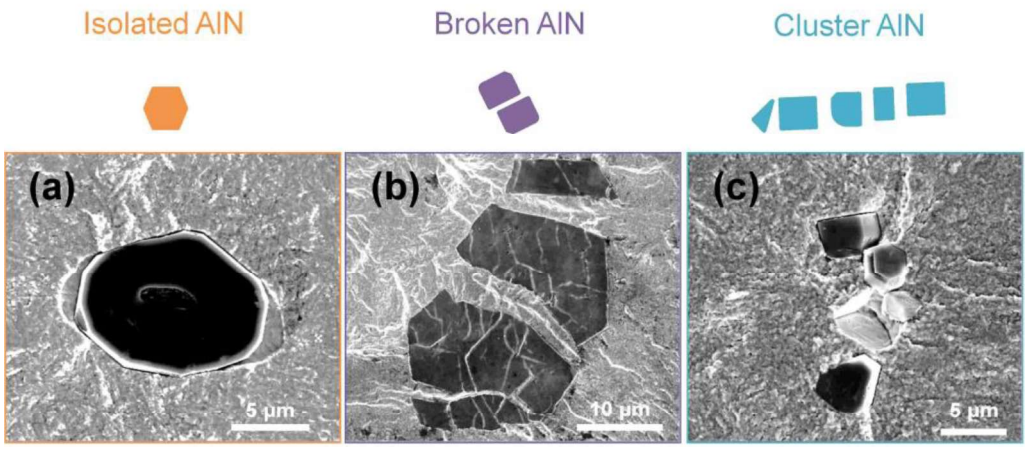

Fig.4. SEM fractography of the three types of inclusion morphologies that lead to fatigue crack initiation **(a)** Isolated AlN particle **(b)** Broken AlN particle **(c)** Cluster of AlN particles

The dominant type of inclusion leading to crack initiation in fatigue is the isolated AlN inclusion.

3.3 Quantitative fractography and interpretation with Linear Elastic Fracture Mechanics (LEFM):

To interpret the scatter in fatigue life and, in particular, the contribution of the different fatigue propagation stages to the fatigue life, LEFM has been applied for the characteristic stages of fatigue crack propagation. It used the results of quantitative fractography. Two

batches of specimens tested in fatigue at 20°C were investigated: one batch of specimens was tested at a mean stress value of σ_{max} ≈1450 MPa. The second batch corresponded to specimen tested at a lower stress of σ_{max} ≈1300 MPa. The latter was chosen in order to increase chances of finding a FGA by fractography. As stated in the literature **[19]**, the FGA is supposed to increase in size for lower applied stresses as the stress intensity factor at the FGA border was found to be constant for a given material and temperature. Collected fractography data on the sizes of inclusions, FGA, fish-eye and end of the fatigue crack growth were used to interpret with LEFM crack initiation and propagation. Each stage of the crack micro-propagation was evaluated with critical values of stress intensity factor range calculated according to Murakami's equations: $\Delta K_{max} = 0.50 \times \sigma_{max} \times \sqrt{(\pi \sqrt{(a)})}$ for internal crack initiation mode and $\Delta K_{max} = 0.65 \times \sigma_{max} \times \sqrt{(\pi \sqrt{(a)})}$ for the surface crack initiation mode. σ_{max} corresponds to the applied maximum tensile stress (and also the stress range as the stress ratio is 0 here); experimental σ_{max} of tested specimens were used to calculate stress intensity factor values, and a corresponds to the projected cross section area of the crack zone on the fracture surface perpendicular to the applied stress axis **[7]**.

The use of LEFM for small cracks is questionable. Even if fatigue tests were conducted in the elastic domain, around inhomogeneities as inclusions, it is possible to reach the plastic domain. Therefore short crack like crack initiation on the inclusions or micropropagation in the FGA, occurs in a domain where LEFM is not fully appropriate as the plastic zone has a similar size to that of the very short cracks. Moreover, the K value for the inclusion is approximate due to its complex shape. Feret diameters can be used to calculate the particle area and subsequently stress intensity factor, but those dimensions do not include inclusion's shape that can affect the value. But still, many papers **[1, 17-20, 24]** have used LEFM to describe fatigue crack propagation and it seems to capture well the main driving forces of the crack.

Fig.5 gives a schematic representation of the four stages of crack propagation for internal crack initiation. K_{inc} is the stress intensity factor caused by the inclusion represented in blue. It is assumed that the inclusion is fractured at the beginning. $K_{FGA/th\ fish\text{-}eye}$ corresponds to the transition between the end of FGA's formation and the beginning of the propagation under vacuum in the fish-eye. The stress intensity factor for FGA formation is represented schematically in red. $K_{Fish\text{-}eye/air\ propagation,}$ in green, is the transition of the crack between the end of the fish-eye and the propagation under air. The last stage, in black, corresponds to stress intensity factor at the end of the crack growth.

For each of these stages Murakami's equations were used to determine the stress intensity factor, with the a corresponding to the projected cross section area of a crack stage. For example, to determine $K_{FGA/th\ fish\text{-}eye}$, the $\sqrt{(a)}$ corresponds to the equivalent diameter of the FGA zone, and for $K_{FGA/th\ fish\text{-}eye,}$ the $\sqrt{(a)}$ corresponds to the equivalent diameter of the fish-eye circle.

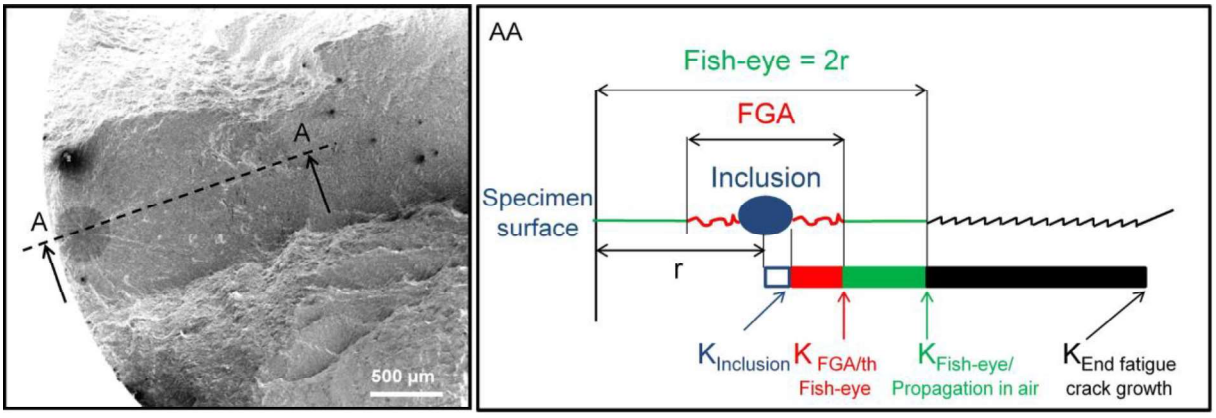

Fig.5. Schematic representation of the stages of crack initiation and propagation. Critical crack lengths at the end of each stage are interpreted with LEFM and the associated stress intensity factors

Fig.6 is a diagram of stress intensity factors at each stage for 28 specimens tested at room temperature. Borders between two colours correspond to critical stress intensity factor values of a crack propagation stage.

Specimens are ranked in terms of fatigue lifetime with the last specimen n°28 having the longest lifetime. Specimens having a shaded area n°1 to n°12 and n°14, 15 and 17 correspond to a surface crack initiation mode while the other specimens correspond to an internal crack initiation mode. In the latter case, they can be easily distinguished with the red and green domains corresponding respectively to a FGA and fish-eye formations. Results show that FGA is not present for surface crack mode and not systematically present in the internal crack initiation mode, but only exists for the longest fatigue lifetimes. Moreover, it appears that the stress intensity factor at the end of the FGA formation is a *constant* threshold value around 7 MPa√m, regardless the applied stress. This is consistent with the findings by **[1, 12, 18, 23]**. It can also be seen that K_{inc} decreases with increasing lifetimes. At a constant applied stress it means that small inclusion sizes lead to long fatigue lives. Thus, small inclusions leading to K_{inc} below the K_{FGA} threshold value, can lead to the formation of FGA. On the other hand, no formation of FGA is expected for larger inclusions with K_{inc} higher than 7 MPa√m, such as for specimens n°18, 19 and 20. Formation of FGA around inclusions is a dominant factor for the long fatigue lifetime and seems to be affected by an environmental effect as they cannot be found for surface initiations even though very low K_{inc} values can be found for surface initiations. It can also be concluded that the formation of the fish-eye alone (green), without FGA formation, does not substantially affect the fatigue lifetime.

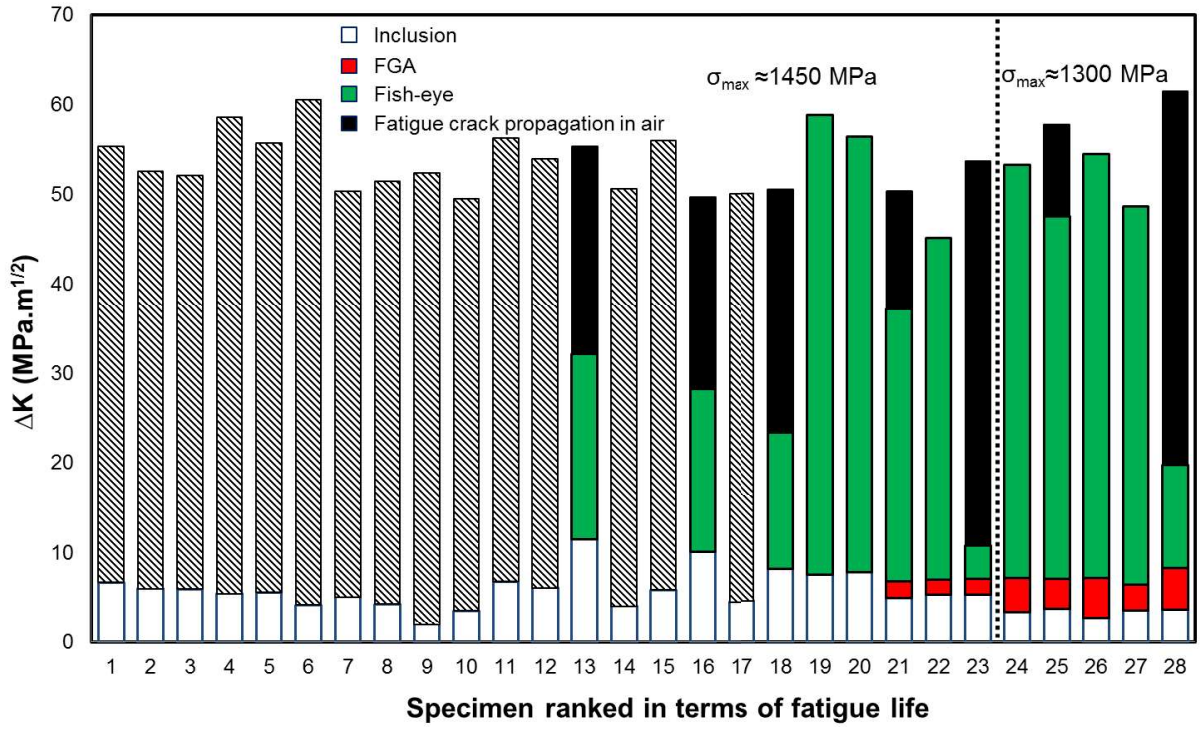

Fig.6. ΔK values calculated with LEFM for each stage of the crack propagation for 28 specimens tested in fatigue at 20°C (Specimens n°1 to n°23 were tested at σ_{max} ≈1450 MPa; specimens n°24 to n°28 were tested at σ_{max} ≈1300 MPa). Surface crack initiation samples are shown with a shaded area.

3.4. Mechanisms of FGA formation

After an investigation on FGA formation conducted using several SEM fractography observations, results in **Fig.7** suggest that FGA formation is a gradual process occurring in a very small process zone, most likely the plastic zone. We come to this conclusion as the FGA crack propagation was stopped by the incoming air at the specimen surface, see **Fig.7 (c).** This effect is clearly illustrated in **Fig.7 (c),** where a FGA was formed equally around the entire particle with a diameter corresponding to its distance to the specimen surface. This environmental effect is also consistent with the results by Spriestersbach **[16]** where a FGA could be generated from a FIB (Focus Ion Beam) defect, but only in vacuum and not in air.

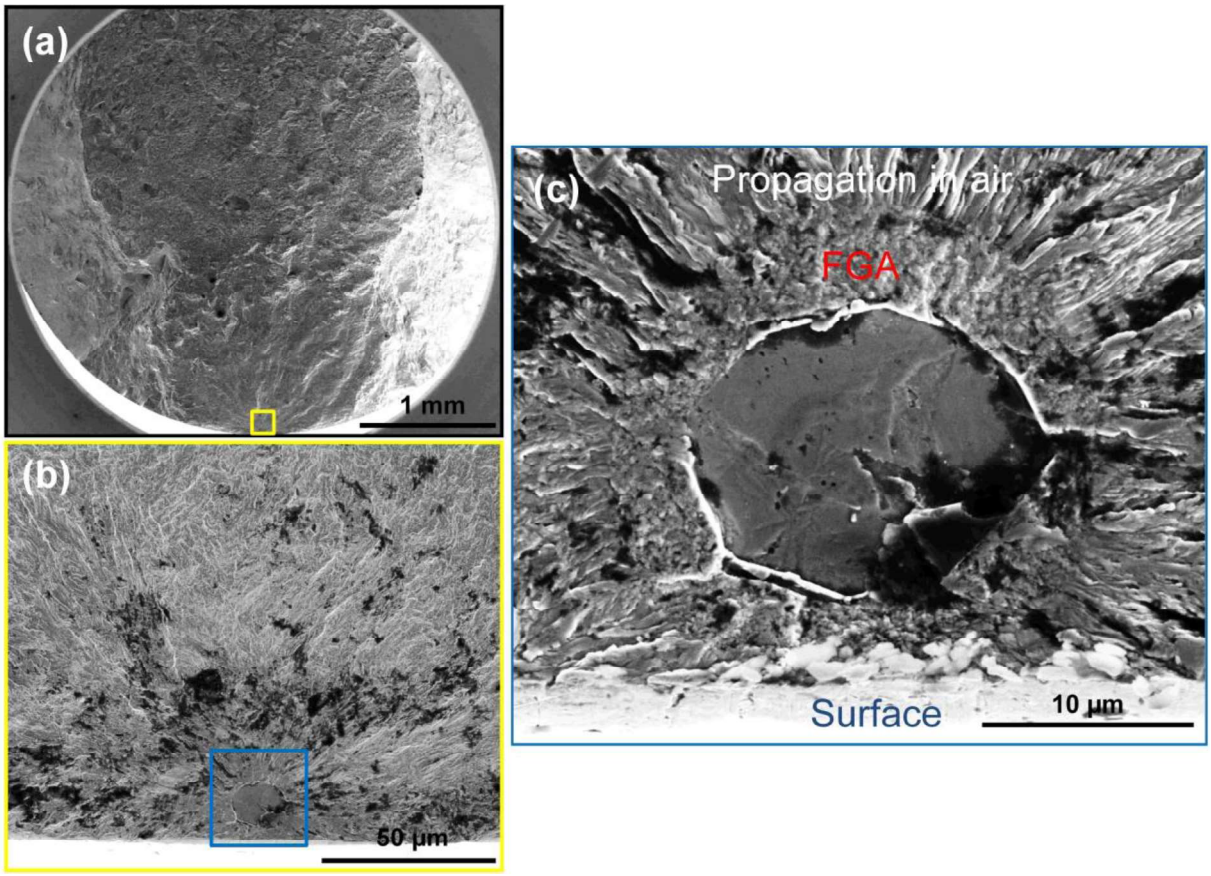

Fig.7. SEM fractography showing a propagating FGA which was stopped by the incoming air at the specimen surface. (a) Fatigue fractography of an internal crack initiation mode. (b) Zoom on crack initiation on an AlN inclusion at the subsurface. (c) Zoom on FGA around the inclusion

This finding highlights strong similarities between FGA formation and a stage-I like crack propagation with a crystallographic character.

These similarities are:

1. The environmental effect on the FGA formation and its propagation (i.e. vacuum is needed);
2. The granular (most likely crystallographic) faceted fracture surface and;

3. Its occurrence for low values of K and small associated plastic zone sizes compared to grain sizes.

In the case of crystallographic crack propagation, the instantaneous process zone of the FGA formation and potential microstructure refinement for martensitic steels is the plastic zone. This interpretation is on the one hand similar to the scenario proposed by Sakai et al. **[1]** who also suggested that the FGA formation is a gradual process in a vacuum. On the other hand, the difference is that he suggested that this process ocurred over some distance, typically up to the FGA radius, from the cracked particle. This distance is an order of magnitude longer than the theoretical plastic zone radius that we believe to be the process zone size.

As a reminder: *Stage I*, in contrast to stage I-like propagation, is identified *in single crystals* with a crack growing in a plane inclined at an angle *about 45*° with respect to the load axis. It is also typical of the *early propagation of micro-cracks in surface grains* as initially shown by Forsyth **[25]**, also see **[27]**.

Stage I-like crystallographic crack propagation in *polycrystalline* materials corresponds to:

1. stage I propagation at the scale of each individual grain along the crack path. At the macroscopic scale, however, the crack propagates normal to the stress axis **[27]**.
2. This crystallographic crack propagation stage can be formed at very low ΔK levels and is associated with *a crack-tip plastic zone which must remain confined within a few grain diameters* **[25-27]**.
3. It occurs in a *vacuum or dry air* environment and can be identified with facetted morphology **[25-27]**.

This stage is described in *Petit et.al* as a stage I propagation at the scale of each individual grain along the crack front with a high sensitivity to microstructure and related slip

localization in individual grains **[27]**. As a consequence of shielding effects (crack deviation and microstructural barriers), the growth of a crack during this stage is greatly retarded compared to a stage II propagation **[27]**. A fish eye and crystallographic area formation during fatigue of Inconel 718 had also been identified, in *Abikchi et.al.* **[29]**. The crystallographic zone in Inconel 718 appears with a different morphology than that which is usually found for martensitic high strength steels. The crystallographic zone formed around an inclusion inside a fish-eye has a grain size of 7 µm **[29]**. The larger the microstructural entity that governs the cyclic slip activity (e.g. grain size) the larger the crystallographic zone. Stage I-like crack propagation has also been found for near threshold propagation in (bcc) Armco iron in **[30]**. Near the threshold the crack propagates over short distances along crystallographic planes. This causes a faceted fracture surface.

For the martensitic steel studied here, it is very hard to verify the cracking along crystallographic planes as the crystals are extremely small (less than 1µm). The granular character of the FGA fracture surface, however, is consistent with a crystallographic cracking.

In the literature, several authors suggest that a load ratio of -1 is needed to obtain a FGA , e.g. **[31]**. Here a load ratio of 0 is applied and a clear FGA formation is still found. This implies that a load ratio of -1 may not be necessary to obtain a FGA. Locally, however there might occur some compression in the crack wake due to crack closure for a macroscopic load ratio of 0. As the crack is short, though, during FGA formation, the compressive stresses due to crack closure should remain limited.

Following the idea that FGA formation has strong analogies with crystallographic, stage I-like, crack propagation in a vacuum, the plastic zone size at the crack tip must correspond to the lengths of a few microstructural entities. To clarify this aspect, sizes of plastic zone at the crack tip of FGA were calculated using fractography expertise data in **fig.6** for the two applied stress levels. Irwin's equation (**Eq.1**) of the plastic zone size r_p was used in cyclic

loading **[26]**. Yield strength (σ_y) at 20°C and stress intensity factor of FGA calculated for each specimen presenting a FGA was used to determine the plastic zone size.

$$r_{p,cyclic} = \frac{1}{4\pi} \times \left(\frac{K_{FGA}}{\sigma_y}\right)^2$$

Equation 1: Irwin approximation of the cyclic plastic zone size at crack tip of FGA in cyclic loading **[26]**

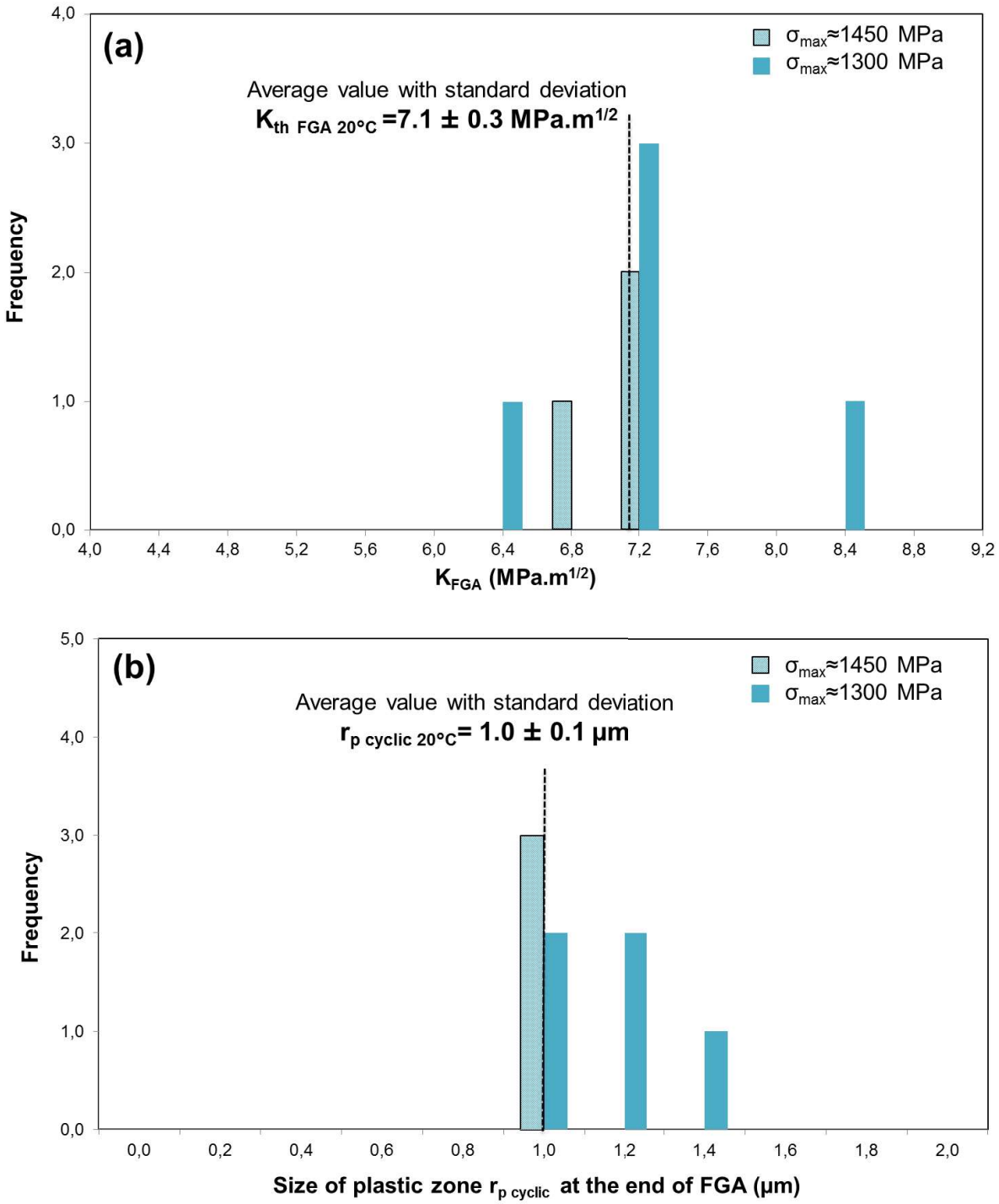

Fig.8. Histogram of (a) K values at the FGA border and corresponding (b) size of the cyclic plastic zone at crack tip for a constant loading at 20°C

Results presented in **fig.8** show a constant $r_{p,cyclic}$ value at the FGA crack tip around 1 µm ± 0.1 µm for specimens with FGA for two applied stress levels. Plastic zone size of FGA

corresponds approximately to a microstructural dimension of a martensite lath length or three times the lath width which seems to govern the end of FGA formation. According to the definition given previously, a strong analogy can be identified between FGA formation and crystallographic stage I-like crack propagation.

However, in the equation (**Eq.1**), the plastic size zone of FGA is correlated to its stress intensity factor. Thus to verify that $r_{p\ FGA}$ is a constant value and depends only of the material microstructure no matter the applied conditions, it is necessary to decouple r_{pFGA} from K_{FGA}. This can be achieved performing tests at higher temperature to diminish the yield strength but keep the material grain structure the same and then evaluate the r_p value. Fatigue specimens were tested at 400°C at a maximum stress level close to that used for specimens at 20°C. The reasoning proceeds with a comparison at 20°C and 400°C based on fractography and fracture mechanics as follows:

The hypothesis for the transition between stage I-like and stage II crack propagation is to reach a plastic zone size that is equal to a characteristic microstructural entity size that governs the cyclic plastic slip:

$$r_{p\ 20°C,cyclic} = r_{p\ 400°C,cyclic} = \text{constant} = \text{lath length (or } 3 \times \text{lath width)}$$

Using its link to the stress intensity factor and yield stress we obtain:

$$\frac{1}{\pi} \times \left(\frac{KFGA\ 20°C}{2\sigma_{y\ 20°C}} \right)^2 = \frac{1}{\pi} \times \left(\frac{KFGA\ 400°C}{2\sigma_{y\ 400°C}} \right)^2 \textbf{(Eq.2.a)}$$

This equation simplifies to:

$$\frac{K_{FGA\ 20°C}}{\sigma_{y\ 20°C}} = \frac{K_{FGA\ 400°C}}{\sigma_{y\ 400°C}} \textbf{(Eq.2.b)}$$

Using the following ratio for the yield stress at different temperatures (Yield stress values at 20°C and 400°C were measured from experiment and the ratio is given below):

$$\frac{\sigma_{y\,400°C}}{\sigma_{y\,20°C}} \approx 0.75 \text{ (Eq.2.c)}$$

We transform (**Eq.2.b**) and obtain a theoretical factor between the critical stress intensity factors at the end of the FGA for the different temperatures:

$$0.75\ K_{FGA\,20°C} = K_{FGA\,400°C} \text{ (Eq.2.d)}$$

This means for the FGA sizes for the different temperatures (simplifying Murakami's equation **[7]**):

$$0.75 \sqrt{\sqrt{area_{FGA\,20°C}}} = \sqrt{\sqrt{area_{FGA\,400°C}}} \text{ (Eq.2.e)}$$

And, as a consequence, for the FGA diameter:

$$0.56 \sqrt{area_{FGA\,20°C}} = \sqrt{area_{FGA\,400°C}} \text{ (Eq.2.f)}$$

Equation 2: Comparison of FGA sizes for 20°C and 400°C based on a constant FGA plastic zone size

If $r_{p\ FGA,cyclic}$ is a constant value, as supposed, it results that FGA diameter for specimens tested at 400°C should theoretically be 56% of the FGA size of the specimen tested at 20°C, if all other processes remain unchanged by the increase temperature. As a consequence, K_{FGA} would only be constant for isothermal fatigue tests and therefore it should be decreasing when the temperature is increasing.

In order to validate this hypothesis, a fractography study was carried out for specimens tested at 400°C with maximum stress levels close to those applied at 20°C. Results of FGA diameters are presented in **Table 2**. There was some scatter in the values of FGA at 400°C. However, the FGA was clearly smaller at higher temperatures and given stress level than at

room temperature. The ratio between FGA diameter at 20°C and 400°C corresponds to about 60% in average, which is close to the theoretical ratio in **Eq.2**.

Fig.9, fig.10 and **fig.11** show SEM fractography for samples which showed a FGA. In **fig.9** FGA was formed at the principal crack initiation for a tested specimen at 20°C. In contrast, in **fig.10** and **fig.11**, FGA was formed only for secondary crack initiation for tested specimen at 400°C. No FGA was observed around the inclusion in the primary crack as shown in **fig.10 (b)**. This is consistent with the fact that the stress intensity factor generated by the main inclusion (initiating the main crack) was too high to generate a FGA as the associated plastic zone size was larger than 3 microstructural entities (i.e. 3 x lath width or lath length) at high temperature. The secondary cracks were in competition with the primary crack, but as an FGA was formed around smaller particles, the secondary crack was consequently slower than the primary crack. The FGAs measured for specimen tested at 400°C is smaller than specimen tested at 20°C.

Table 2: Results of fractography expertise on specimen tested at 20°C and 400°C

T(°C)	Specimen	σ_{max} (MPa)	FGA diameter (μm)
20	1	1458	31
	2	1447	33
	3	1395	36
400	4	1238	17
	5	1316	17
	6	1486	24
	7	1471	22

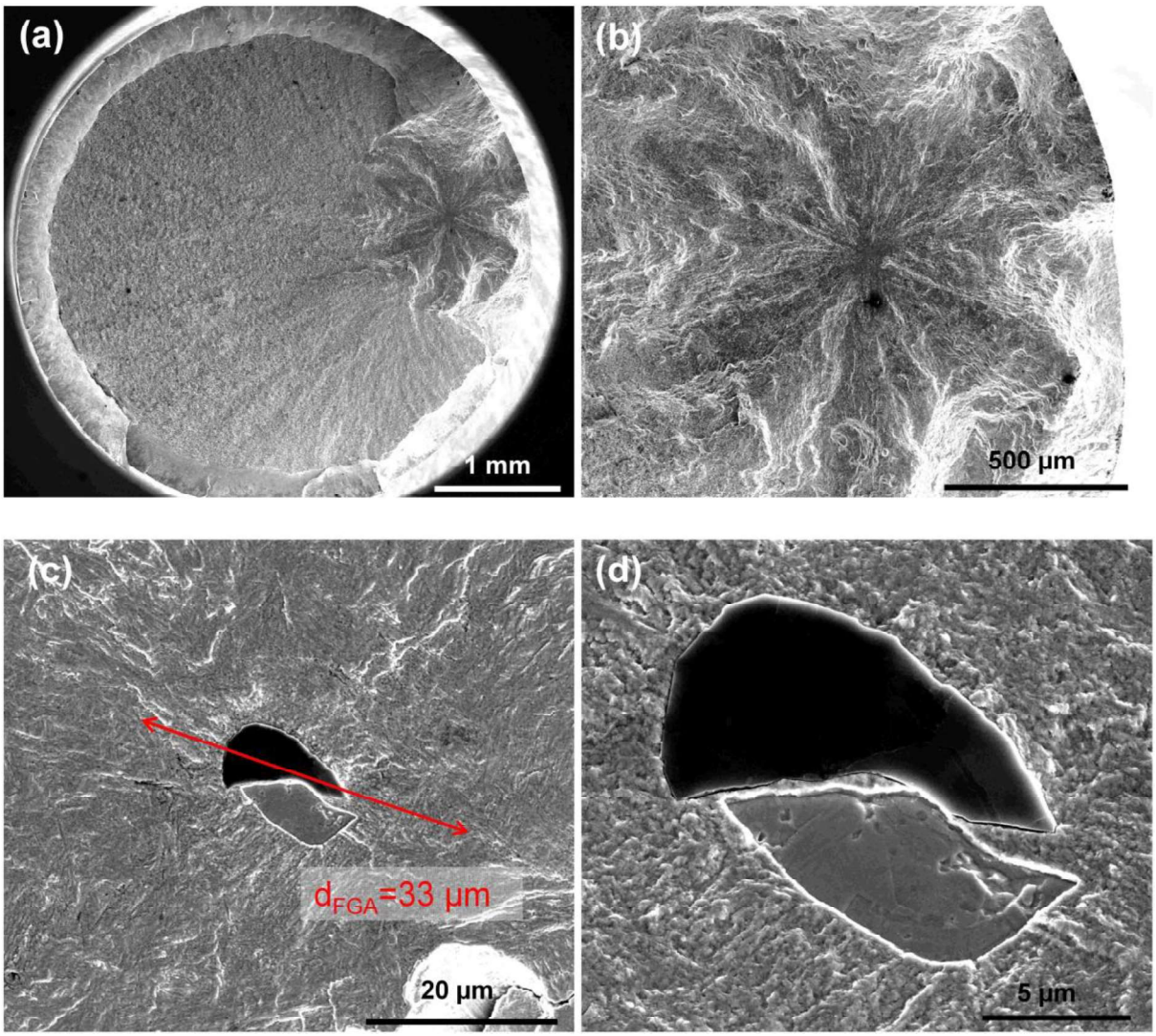

Fig.9: SEM fractography for specimens tested at 20°C with formation of a 33 µm FGA diameter around an AlN inclusion (specimen n°**2** in **Table 2**)

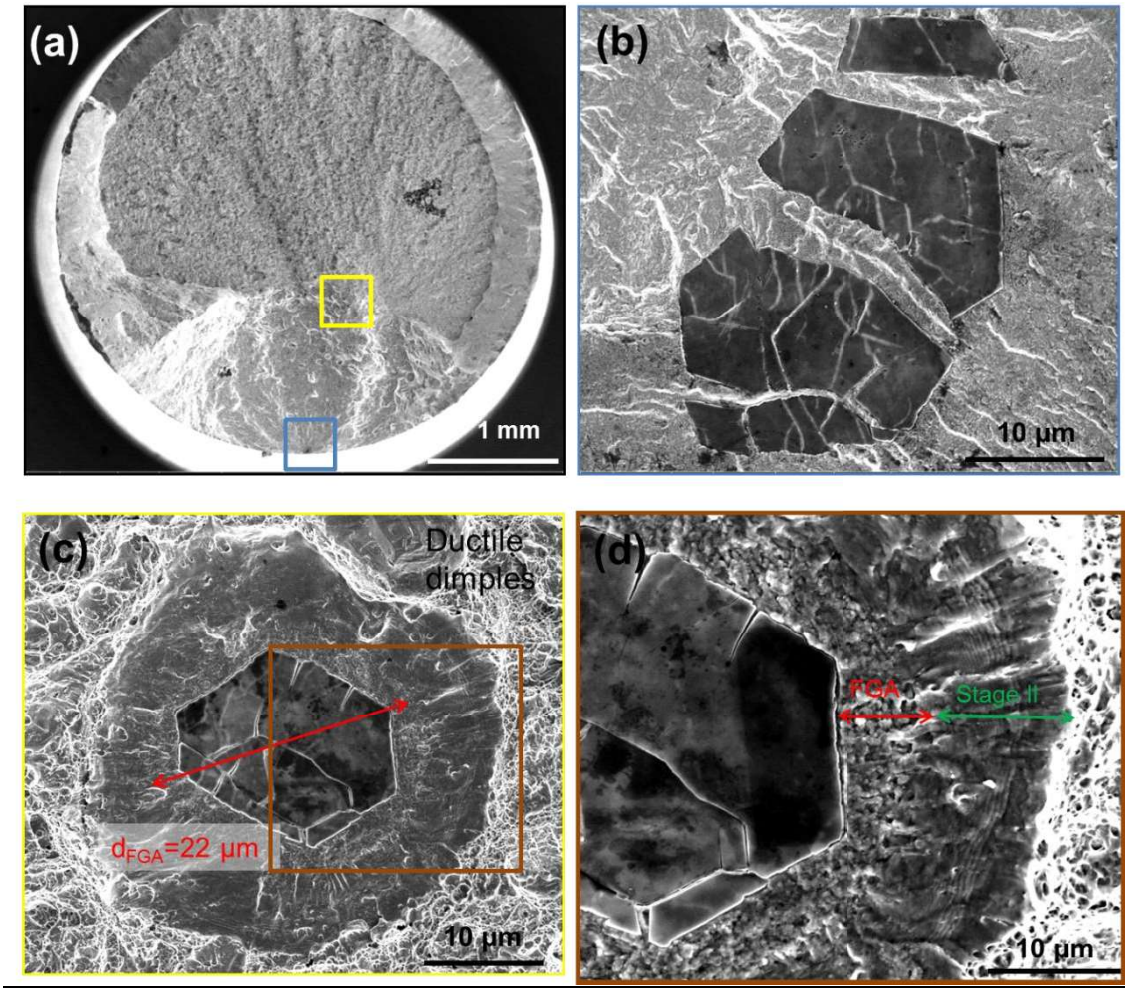

Fig.10. SEM fractography of a (a) specimen tested at 400°C (specimen n°**7** in **Table 2**): (b) principal crack initiation particle without FGA and (c) (d) secondary crack initiation particle with a 22 µm FGA diameter

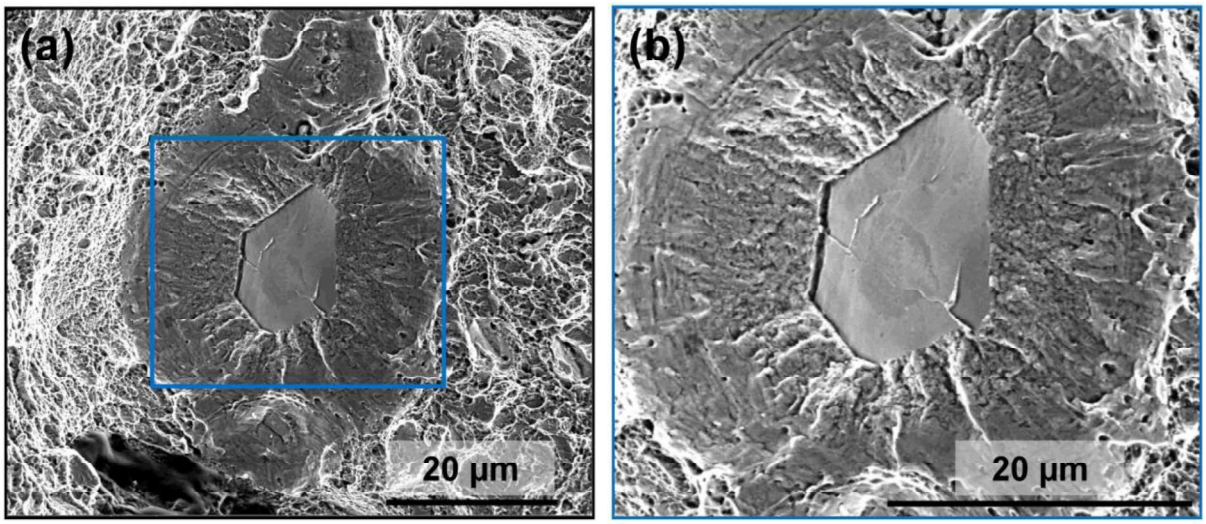

Fig.11. SEM images of a (a) secondary crack initiation fatigue in a specimen tested at 400°C (specimen n°**6** in **Table.2**) (b) Zoom around the inclusion with a 24 µm FGA diameter

A histogram of the evolution of stress intensity factor generated by the FGA with temperature and their corresponding plastic zones size are presented in **fig.12**. Average K_{FGA} values decreased when the temperature is increased. A ratio value of 71% can be found between K_{FGA} values at 20°C and 400°C as it is described in **Eq.2.d**. In contrast, there is no notable change in $r_{p,\ FGA}$ with temperature. The $r_{p,\ FGA}$ value remains constant for the different temperatures around 1.0 µm ±0.2 µm even with different stress levels, as it was suspected. Thus, $r_{p,\ FGA}$ is linked to a microstructural entity, i.e. martensitic lath length (or 3 times its width).

This result confirms that the FGA formation corresponds to a stage I-like crack propagation with crystallographic character and suggests a new scenario for FGA formation.

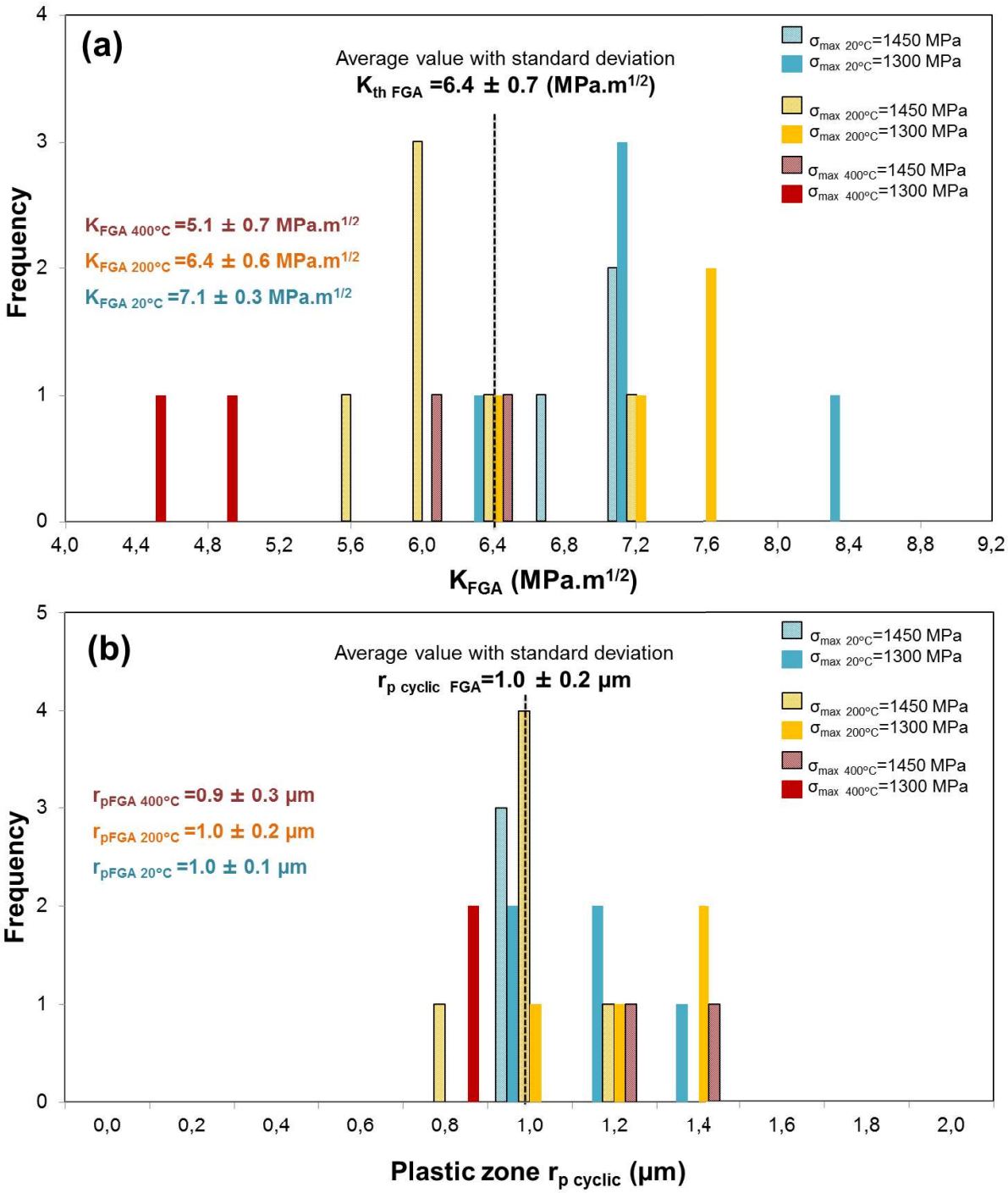

Fig.12. Histogram of (a) K_{FGA} values calculated for two applied stress levels for each temperature (20°C, 200°C and 400°C). Corresponding (b) size of plastic zone at FGA crack tip

3.5 A new scenario of FGA formation

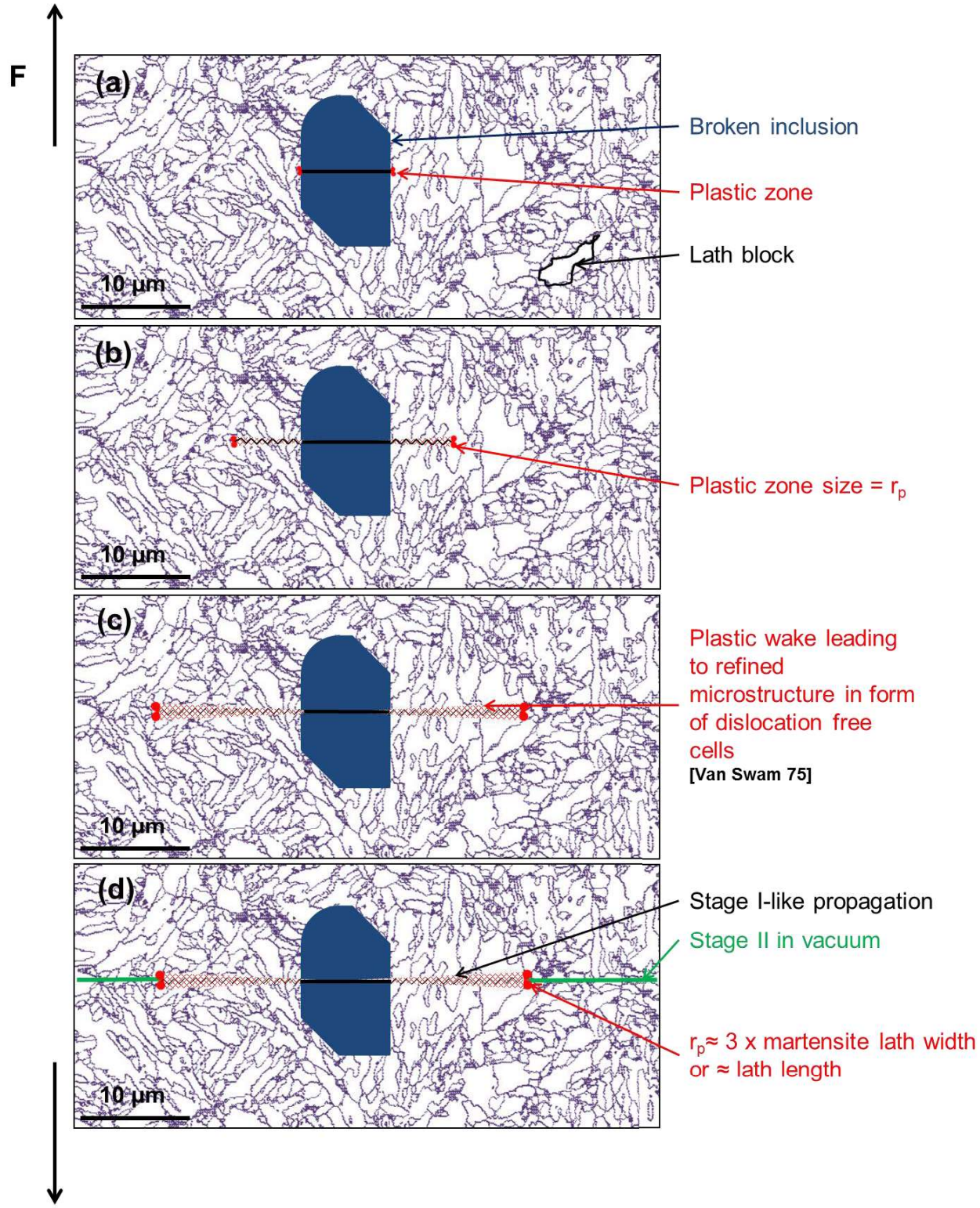

Fig.13. Schematic representation of FGA formation under cycling loading

Following the results shown in earlier sections, a new FGA formation scenario is

schematically presented in **Fig.13**. The fatigue crack initiates from broken non-metallic inclusions due to stress concentration during cyclic loading. The particle is supposed cracked at the start of cyclic loading, which may not be always true. However, elastic modulus differences between particles and matrix and complex particle shapes may already create a sufficient stress intensity to initiate a crack. A plastic zone is formed at the crack tip smaller than a martensite lath length (or 3 x the lath length). The crack propagates slowly and gradually under a stage I-like regime for interior crack initiation with stress intensity factors smaller than $K_{th\ FGA}$, leaving a plastic wake behind. Timewise crack arrests may also occur under such stage I-like propagation. The fine granular aspect of FGA is formed during stage I-like crack propagation through microstructural barriers of martensitic laths. Apparent 'grain refinement' in the FGA is different from classical stage I-like crack propagation **[27]**. In this context and for the discussion of the findings in the literature, the work of *Van Swam et.al.,* which was focused on cyclic softening in maraging steels during cyclic loading, showed the comparison of martensitic microstructure before and after a cyclic deformation **[32]**. Prior to cyclic loading, high dislocation density was observed in the microstructure due to the martensitic transformation. In contrast, after cyclic loading, the microstructure went through a rearrangement of dislocations in clearly defined dislocation free cells during cyclic deformation. Cells arrangement was also mentioned by *Sakai et.al*. during a FGA formation **[1]**. In other words, the microstructural evolution during cyclic loading that is perceived as 'grain refinement' may actually consist of a rearrangement of dislocations in clearly defined cells which is a well-known phenomenon for martensitic steels under cyclic deformation **[32]**. The particularity here is that the plastic zone for crack initiation is initially very small so that the microstructure refinement can only occur in a very small zone (in the order of 1 μm in diameter) and only if the crack is slow enough to subject the same material point to a sufficient number of cycles to refine the microstructure.

When the plastic zone size at the crack tip equals to a martensite lath length, or three times the martensite lath width, the crack switches to a stage II regime under vacuum, creating a fish-eye crack (see **Fig.13c)**. The faster crack propagation in stage II may no longer allow the microstructure to be refined in the plastic zone.

4. Conclusions

Scenarios of surface and internal crack initiation mechanisms have been interpreted using linear elastic fracture mechanics for a high strength martensitic steel. Fatigue cracks systematically initiated at particles. Surface crack initiation led to lower fatigue lives than internal crack initiation. For internal crack initiation, a FGA (Fine Granular Area) was found for long fatigue lifetimes.

The following conclusions on FGA formation can be drawn:

- Initiation at small inclusions which generate a $K_{inclusion}$ smaller than a critical value $K_{FGA/th\ Fish\text{-}eye}$ are needed to generate a FGA.
- FGA formation was found for specimens tested at R_σ=0 in the high cycle fatigue regime.
- Using the Irwin's equation for the cyclic plastic zone size, a *constant plastic zone size* was found at the end of the FGA for different temperatures (20°C, 200°C and 400°C)
    - $\boxed{r_{p,FGA\ 20°C} = r_{p,FGA\ 200°C} = r_{p,FGA\ 400°C}}$
- The characteristic plastic zone size at the end of the FGA corresponded to a martensitic lath length or three times the martensite lath width. This critical plastic zone size was the same for each specimen with a FGA regardless the fatigue testing conditions.
- In contrast, different K_{FGA} values were found for the different temperatures

- $\boxed{K_{FGA\ 20°C} > K_{FGA\ 200°C} > K_{FGA\ 400°C}}$

- FGA formation has strong similarities with a stage I-like crystallographic crack propagation regime. This regime occurs for low stress intensity factors, generating plastic zones sizes smaller than a couple of grains, and under vacuum. FGA formation is a dominant factor for long fatigue lives as stage I-like crack propagation is very slow and strongly affected by microstructural barriers (As a reminder: stage I, in contrast to stage I-like propagation, is identified in single crystals with a crack growing in a plane inclined at an angle about 45° with respect to the loading direction. It is also typical of the early propagation of micro-cracks in surface grains as initially shown by Forsyth **[25]**).

- The microstructural refinement found in the FGA for many martensitic steels in the literature is not classical for stage I like cracking but can be interpreted with a well-known result for martensitic steel, i.e. cyclic loading with generalized plasticity leads to the rearrangement of dislocations, stemming from martensitic transformation, in defined dislocation free cells **[32]**. This is likely to happen in the plastic zone during stage I-like crack propagation, i.e. for FGA formation.

Acknowledgments

The authors would like to acknowledge Safran Aircraft Engines and SafranTech for the financial and technical supports. Alexandre Seror, , Arnaud Longuet, Laurent Ferrer, Alain Köster and Fabrice Gaslain are also thanked for their contribution to this work.

References

[1] Sakai T, Oguma N, Morikawa A. Microscopic and nanoscopic observations of metallurgical structures around inclusions at interior crack initiation site for a bearing steel in very high-cycle fatigue; Fatigue Fract Engn Mater Struct 2015;00: 1-10

[2] Naito T, Ueda H, Kikuchi M. Fatigue behavior of carburized steel with internal oxides and non-martensitic microstructure near the surface, Metallurgical Transactions A 1984; 15: 1431-1436

[3] Murakami Y, Nomoto T, Ueda T. Factors influencing the mechanism of superlong fatigue failure in steels, Fatigue Fract Engng Mater Struct 1999; 22: 581–590

[4] Li Y-D, Zhang L-L, Fei Y-H. On the formation mechanisms of fine granular area (FGA) on the fracture surface for high strength steels in the VHCF regime, International Journal of Fatigue 2016; 82: 402–410

[5] Mughrabi H. Microstructural mechanisms of cyclic deformation, fatigue, crack initiation, and early crack growth, The Royal Society, Phil Trans; 2015; A373: 1-21

[6] Sakai T, Sato Y. Characteristics S-N properties of high carbon chromium bearing steel under axial loading in long life fatigue; Fatigue Fract Engn Mater Struct 2002; 25: 765-773

[7] Murakami Y. Metal Fatigue: Effects of Small Defects and Nonmetallic Inclusions, Elsevier Book Oxford; 2002

[8] Shiozawa K, Morii Y, Nishino S. Subsurface crack initiation and propagation mechanism in high-strength steel in a very high cycle fatigue regime, International Journal of Fatigue 2006; 28: 1521–1532

[9] Ochi Y; Matsumura T. High-cycle rotating bending fatigue property in very long-life regime of high-strength steels, FFEMS 2002; 25: 823-830

[10] Li W, Wang P. Evaluation of Threshold Condition of Interior Annular Crack Growth in Gigacycle Regime, Applied Mechanics and Materials 2014; 459: 65-69

[11] Grad P, Reuscher B, Brodyanski A. Mechanism of fatigue crack initiation and propagation in the very high cycle fatigue regime of high-strength steels, Scripta Materialia 2012; 67: 838–841

[12] Chai G, Forsman T, Gustavsson F. Formation of fine grained area in martensitic steel during very high cycle fatigue, Fatigue Fract Engn Mater Struct 2015; 38: 1315-1323

[13] S. X. Li. Effects on inclusions on very high cycle fatigue properties of high strength steels, International Materials Reviews 2012; 57: 92-114

[14] Li Y-D, Zhang L-L. On the formation mechanisms of fine granular area (FGA) on the fracture surface for high strength steels in the VHCF regime, International Journal of Fatigue 2015; 82: 402-410

[15] Nakamura T, Oguma H, Shinohara Y. The effect of vacuum-like environment inside sub-surface fatigue crack on the formation of ODA fracture surface in high strength steel, Procedia Engineering 2010; 2: 2121–2129

[16] Spriestersbach D, Brodyanski A, Lösch J, Kopnarski M, Kerscher E. Very high cycle fatigue of high-strength steels: Crack initiation by FGA formation investigated at artificial defects, Structural Integrity Procedia ECF21, 2016

[17] Hong Y, Lei Z. Propensities of crack interior initiation and early growth for very-high-cycle fatigue of high strength steels, International Journal of Fatigue 2014; 58: 144–151

[18] Zhao A, Xie J, Sun C. Effects of strength level and loading frequency on very-high-cycle fatigue behavior for a bearing steel, International Journal of Fatigue 2012; 38: 46–56

[19] Ogawa T, Stanzl-Tschegg S.E, Schönbauer B.M. A fracture mechanics approach to interior fatigue crack growth in the very high cycle regime, Engineering Fracture Mechanics 2014; 115: 241–254

[20] Stanzl-Tschegg S.E, Schönbauer B.M. Near-threshold fatigue crack propagation and internal cracks in steel, Procedia Engineering 2010; 2: 1547–1555

[21] Kitahara H, Ueji R. Crystallographic features of lath martensite in low carbon steel, Acta materialia 2006; 54: 1279-1288

[22] Feret, L. R. Assoc Int pour l'Essai des Mat 1932 ; 2D : 428–436

[23] Schönbauer B.M, Stanzl-Tschegg S.E. Influence of environment on the fatigue crack growth behaviour of 12% Cr steel, Ultrasonics 2013; 53: 1399–1405

[24] Le Jolu T, Morgeneyer T-F, Denquin A, Gourgues-Lorenzon A-F. Fatigue lifetime and tearing resistance of AA2198 Al-Cu-Li alloy Friction Stir Welds: Effect of defects, International Journal of Fatigue 2015; 70: 463-472

[25] Forsyth P.J.E, A two stage process of fatigue crack growth, Crack Propagation: Proceedings of Cranfield Symposium, London: Her Majesty's Stationery Office, 1962; 76–94

[26] S. Suresh. Fatigue of Materials Second Edition, Cambridge University Press, 1998

[27] Petit J, Sarrazin-Baudoux C, Some critical aspects of low rate fatigue crack propagation in metallic materials, International Journal of Fatigue 2010; 32: 962–970

[28] Alexandre F. Aspect probabilistes et microstructuraux de l'amorçage des fissures de fatigue dans l'alliage INCO 718, Thèse Ecole Nationale Supérieure des Mines de Paris, Mars, 2004

[29] Abikchi M, Billot T, Crepin J, Longuet A, Mary C, Morgeneyer T-F, Pineau A. Fatigue life and initiation mechanisms in wrought Inconel 718 DA for different microstructures, 13th International Conference on Fracture, Beijing, China, 2013;16–21

[30] Pippan R, Threshold and effective threshold of fatigue crack propagation in ARMCO iron I: The influence of grain size and cold working, Materials Science and Engineering 1991, A138: 1-13

[31] Hong Y, Liu X, Lei Z, Sun C. The formation mechanism of characteristic region at crack initiation for very-high-cycle fatigue of high-strength steels, International Journal of Fatigue 2016; 89: 108–118

[32] Van Swam L.F, Pelloux R.M. Fatigue Behavior of Maraging Steel 300, Metallurgical Transactions A, 1975; 6A: 45-54